

# The Widefield Arecibo Virgo Extragalactic Survey I: New structures in the ALFALFA Virgo 7 cloud complex and an extended tail on NGC 4522

ROBERT F. MINCHIN,<sup>1</sup> RHYS TAYLOR,<sup>2</sup> JOACHIM KÖPPEN,<sup>3</sup> JONATHAN I. DAVIES,<sup>4</sup> WIM VAN DRIEL,<sup>5</sup> AND OLIVIA KEENAN<sup>6</sup>

<sup>1</sup>*Stratospheric Observatory for Infrared Astronomy/USRA, NASA Ames Research Center, MS 232-12, Moffett Field, CA 94035, USA*

<sup>2</sup>*Astronomical Institute of the Czech Academy of Sciences, Bocni II 1401/1a, 141 31 Praha 4, Czech Republic*

<sup>3</sup>*Institut für Theoretische Physik und Astrophysik der Universität zu Kiel, D-24098, Kiel, Germany*

<sup>4</sup>*School of Physics and Astronomy, Cardiff University, Queen's Buildings, The Parade, Cardiff, CF24 3AA, United Kingdom*

<sup>5</sup>*GEPI, Observatoire de Paris, PSL Research University, CNRS, 5 place Jules Janssen, F-92190 Meudon, France; Station de Radioastronomie de Nançay, Observatoire de Paris, CNRS/INSU USR 704, Universit d'Orléans OSUC, route de Souesmes, F-18330 Nançay, France*

<sup>6</sup>*School of Physics and Astronomy, Queen Mary, University of London, G O Jones Building, 329 Mile End Rd, London, E1 4NT, United Kingdom*

## ABSTRACT

We are carrying out a sensitive blind survey for neutral hydrogen (HI) in the Virgo cluster and report here on the first  $5^\circ \times 1^\circ$  area covered, which includes two optically-dark gas features: the five-cloud ALFALFA Virgo 7 complex (Kent et al. 2007, 2009) and the stripped tail of NGC 4522 (Kenney et al. 2004). We discover a sixth cloud and low velocity gas that extends the velocity range of the complex to over  $450 \text{ km s}^{-1}$ , find that around half of the total HI flux comes from extended emission rather than compact clouds, and see around 150 percent more gas, raising the total HI mass from  $5.1 \times 10^8 M_\odot$  to  $1.3 \times 10^9 M_\odot$ . This makes the identification of NGC 4445 and NGC 4424 by Kent et al. (2009) as possible progenitors of the complex less likely, as it would require an unusually high fraction of the gas removed to have been preserved in the complex. We also identify a new component to the gas tail of NGC 4522 extending to  $\sim 200 \text{ km s}^{-1}$  below the velocity range of the gas in the galaxy, pointing towards the eastern end of the complex. We consider the possibility that NGC 4522 may be the parent galaxy of the complex, but the large velocity separation ( $\sim 1800 \text{ km s}^{-1}$ ) leads us to rule this out. We conclude that, in the absence of any better candidate, NGC 4445 remains the most likely parent galaxy, although this requires it to have been particularly gas-rich prior to the event that removed its gas into the complex.

*Keywords:* galaxies:clusters:individual (Virgo); galaxies:individual (NGC 4522); radio sources:individual (ALFALFA Virgo 7 complex); radio lines: galaxies

## 1. INTRODUCTION

Virgo has long been a fertile ground for searches for neutral hydrogen (HI) gas unassociated with optical counterparts. These include well known examples such as HI 1225+01 (Giovanelli & Haynes 1989; Giovanelli, Williams & Haynes 1991; Chengalur, Giovanelli & Haynes 1995) and VIRGOHI 21 (Davies et al. 2004; Minchin et al. 2005, 2007; Haynes, Giovanelli & Kent 2007) that are extended sources with  $M_{\text{HI}} \sim 10^8 - 10^9 M_\odot$ , as well as many other clouds revealed in recent years, primarily by the Arecibo Legacy Fast Arecibo L-

band Feed Array (ALFALFA) survey (Kent et al. 2007) and the Arecibo Galaxy Environment Survey (AGES) (Taylor et al. 2012). Such dark features may be debris from tidal encounters between galaxies, or they may have their origin in the removal of gas from galaxies via ram pressure stripping by the intra-cluster medium (ICM).

With this in mind, we have begun the Widefield Arecibo Virgo Extragalactic Survey (WAVES). This is an extension of the Arecibo Galaxy Environment Survey (AGES) in the Virgo Cluster, with the specific intention of revealing the low column-density neutral hydrogen (HI) content of the cluster. WAVES is currently covering the right ascension range  $12^{\text{h}}09^{\text{m}}00^{\text{s}} - 12^{\text{h}}49^{\text{m}}00^{\text{s}}$  and the declination range  $09^\circ 00' 00'' - 11^\circ 06' 00''$ , filling

in the gap between the AGES VC1 (Taylor et al. 2012) and VC2 (Taylor et al. 2013) fields to the same sensitivity and spectral resolution as AGES.

The first quadrant of the survey, covering a 5 square degree area over RA  $12^{\text{h}}29^{\text{m}}00^{\text{s}} - 12^{\text{h}}49^{\text{m}}00^{\text{s}}$  and Dec.  $09^{\circ}00'00'' - 10^{\circ}00'00''$ , was completed in March 2018. This takes in the area of the ALFALFA Virgo 7 complex, a dark HI cloud complex discovered by the ALFALFA survey (source 7 in Kent et al. 2007) and identified as consisting of five clouds lying between 400 and  $760 \text{ km s}^{-1}$  (see also our Figure 2). VLA observations (Kent et al. 2009) confirmed two of the clouds (C1 (7c) and C2 (7d)) but did not detect clouds C4 (7b) or C5 (7e) due to their distances from the pointing centre. Cloud C3 (7a) lay outside of the area mapped by the VLA. Sorgho et al. (2017) also covered this region with a combined WSRT and KAT-7 map; they detected cloud C1 but not cloud C4, which should have been detectable based on its single-dish HI mass if it were a point source. The ALFALFA map of Kent et al. (2009, figure 2) shows two of the five clouds in the complex (C1 and C4) to be connected, but the other three clouds are separated at their sensitivity level. They find a total mass for the complex of  $5.1 \times 10^8 M_{\odot}$  at an assumed distance for the Virgo cluster of 16.7 Mpc, equivalent to a total flux of  $7.8 \text{ Jy km s}^{-1}$ . Kent et al. (2009) found that a possible optical counterpart near the C2 cloud, VCC 1357, had a large separation from the VLA position and was thus unlikely to be associated with the complex.

The ALFALFA Virgo 7 complex is thus a unique structure in the Virgo cluster. Only one other HI feature is known which is detached from its parent galaxy – the cloud associated with VCC 1249 (Arrigoni Battaia et al. 2012). However, in that case the cloud is only 14 kpc projected distance from its parent, whereas the nearest plausible parent for the complex (NGC 4445) is separated by  $\sim 180$  kpc in projection from its center. The complex is also amongst the most massive of the streams known in Virgo and has a highly complex internal structure. No other feature in Virgo shows this combination of features. We describe our observations of the complex in Section 3.

This first quadrant also takes in the galaxy NGC 4522, a classic example of ram pressure stripping in the Virgo cluster (Kenney & Koopmann 1999). This has a well-known HI tail, observed by Kenney et al. (2004) and Chung et al. (2007) and simulated by Vollmer et al. (2006). Like the ALFALFA Virgo 7 complex, the tail of NGC 4522 is an example of optically-dark HI gas in Virgo although, unlike the complex, it remains connected to its parent galaxy and the mechanism by which

it has been created is much clearer. We describe our observations of NGC 4522 in Section 4.

All velocities in this paper are radial velocities in the barycentric frame and the optical (*cz*) convention.

## 2. OBSERVATIONS

Observations on this field were made between January 2017 and March 2018 using the Arecibo L-band Feed Array (ALFA). WAVES uses the same scan pattern and data reduction pipeline as AGES (detailed in Auld et al. 2006). As around half of the data were taken prior to Hurricane Maria (20 September 2017), which caused changes to the gain of the Arecibo telescope, and half afterwards, separate cubes were initially made from each half of the dataset and their respective flux calibrations were compared using the fluxes of strong HI sources within the cube. An adjustment of around 8 percent was then made to the post-Maria calibration and the post-Maria data were re-reduced with the new calibration before the final datacube was made.

### 2.1. Verification of the flux scale

We check our calibration by comparing our total HI fluxes to those seen by ALFALFA. There are 33 sources in the ALFALFA catalogue of Kent et al. (2008) within the WAVES quadrant boundary. After removal of HVCs, the extended clouds from the complex, lower quality ('code 2') sources, and sources noted to have issues with their parameter fitting, we are left with 17 sources. Two of these lie too close to the edge of our cube to be well parameterized in WAVES, giving 15 good comparison sources. In Figure 1 we compare our fluxes for these sources to the ALFALFA fluxes from Kent et al. (2008) and the rescaled ALFALFA fluxes from Haynes et al. (2018), which are, on average, 8 percent higher. We find the weighted mean of the ratio of the WAVES flux to the Kent et al. (2008) flux is  $1.07 \pm 0.04$  and for the Haynes et al. (2018) flux is  $0.96 \pm 0.04$ . Our flux scale thus appears to be slightly higher than the initial ALFALFA flux scale, but is consistent with their corrected flux scale.

## 3. THE ALFALFA VIRGO 7 COMPLEX

Around the velocity of the ALFALFA Virgo 7 complex, our observations reach an average noise level of  $0.9 \text{ mJy beam}^{-1}$  at a Hanning-smoothed velocity resolution of  $10 \text{ km s}^{-1}$ , around 3 times deeper than the ALFALFA observations.

Figure 2 shows the moment 0 map of the complex over 440 to  $620 \text{ km s}^{-1}$  with the outer contour at  $3\sigma$  ( $0.18 \text{ Jy km s}^{-1}$ ,  $5 \times 10^{18} \text{ cm}^{-2}$ ), the second contour at  $5\sigma$  ( $0.30 \text{ Jy km s}^{-1}$ ,  $8 \times 10^{18} \text{ cm}^{-2}$ ), and other contours at

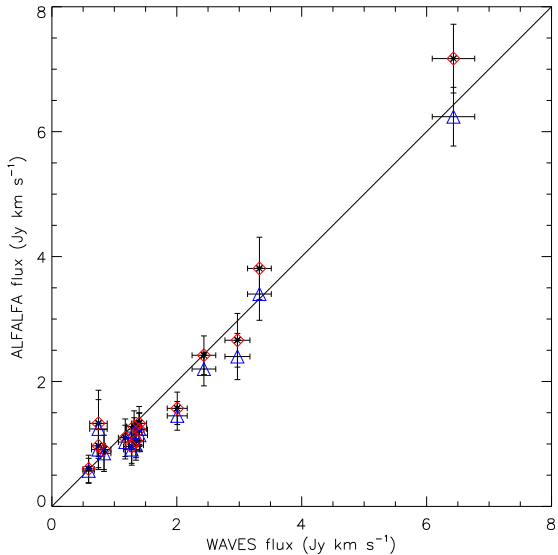


**Figure 1.** Comparison of integrated H I line fluxes (in  $\text{Jy km s}^{-1}$ ) of sources detected in both WAVES and ALFALFA. For ALFALFA, fluxes from Kent et al. (2008) are shown by blue triangles and fluxes from Haynes et al. (2018) are shown by red lozenges. Errors calculated according to the formulae of Koribalski et al. (2004). To guide the eye, the solid line indicates a 1:1 relationship.

increasing steps to bring out the peaks of the clouds. The five clouds identified in the complex by Kent et al. (2007, 2009) can be clearly seen, but we also see a sixth cloud (which we label C6 for consistency with Kent et al. 2009’s nomenclature) between C4 and C2.

Figure 3 shows channel maps averaged over  $55 \text{ km s}^{-1}$  and color-coded by velocity, over the range  $280$  to  $780 \text{ km s}^{-1}$ . It is apparent that, unlike in the map of Kent et al. (2009), at the WAVES sensitivity level the whole complex is joined up by H I bridges. We also see gas down to  $280 \text{ km s}^{-1}$ ,  $120 \text{ km s}^{-1}$  below the lower limit of the gas seen by Kent et al. (2009); this is shown by violet and purple contours in Figure 2. The new cloud C6 is visible in the cyan and green contours, and partly in the yellow contours.

Cloud C4 can be clearly seen to consist of two overlapping components, with a shift in the centre of around  $2.5'$  between the cyan and green contours and the orange and red contours. The higher velocity component has a position (fitted over  $640$  to  $760 \text{ km s}^{-1}$ ) of  $12^{\text{h}}30^{\text{m}}24.0^{\text{s}}$ ,  $09^{\circ}36'50''$  while the lower velocity component has a position (fitted over  $460$  to  $580 \text{ km s}^{-1}$ ) of  $12^{\text{h}}30^{\text{m}}17.7^{\text{s}}$ ,  $09^{\circ}34'40''$ . Spectra of the two components (summed over a  $5' \times 5'$  box) are shown in Figure 4.

Kent et al. (2009) describe cloud C3 as ‘unresolved with the ALFA beam’. However, we see the cloud as being clearly extended along an axis pointing towards C1, with the centre shifting further along this axis (away

from C1) at higher velocities. This can be seen in Figure 5. A bridge between cloud C3 and the main complex can be seen in the blue and cyan contours and in the greyscale on this figure, which covers the same velocity range. The bridge connects to an extension seen at low SNR to the west side of C4 in the Kent et al. (2009) map, which is now seen to be real (conversely, the extension to the northeast side of C4, seen at a very similar flux level in the Kent et al. 2009 map, is not seen in our data). However, in velocity space the connection looks to be to C1 (which would be consistent with the alignment of the axis of cloud C3) rather than to C4.

Clouds C2 and C5 contain lower velocity gas than that seen by Kent et al. (2009), which bridges between the two clouds; this is marginally visible (at around  $2\sigma$ ) in the Kent et al. (2009) spectrum of C2 but is clearly detected here. This is shown in Figure 6. It can be seen that there is detected gas at the positions of C5 and C2, stretching about half way to the position of C6 and with the peak in the  $280$ – $340 \text{ km s}^{-1}$  map about half way between C5 and C2. There is also gas in the main complex, with a peak between the positions of C1 and C4, stretching to the root of the bridge to C3. The gas in this velocity range does not contribute greatly to the total H I content of the complex, with  $F_{\text{HI}} = 0.34 \text{ Jy km s}^{-1}$  (after sidelobe correction, see below), for an H I mass of  $2.3 \times 10^7 M_{\odot}$ , i.e. less than 2 percent of the total H I mass of the complex. Nevertheless, it provides important information on the connections between the clouds.

The ‘bay’ between C2 and C1, south of the new C6 cloud, is not completely filled in at any of the velocity slices, even though almost all of its area is covered at some velocity or other (see Figures 2 and 3). We fit a position for the C6 cloud (using a  $5' \times 5'$  box) of  $12^{\text{h}}30^{\text{m}}46.8^{\text{s}}$ ,  $09^{\circ}34'04''$ . The flux in the single-pixel spectrum at this position is  $0.78 \pm 0.12 \text{ Jy km s}^{-1}$ , with a peak of only  $6 \text{ mJy}$ , making it less than  $3\sigma$  in the Kent et al. (2007, 2009) data, while the beam-corrected flux within the  $5' \times 5'$  box is  $0.97 \pm 0.13 \text{ Jy km s}^{-1}$ . The total flux measured off the moment 0 map within a  $7' \times 8'$  box enclosing C6 is  $1.62 \pm 0.12 \text{ Jy km s}^{-1}$ .

### 3.1. Total H I content of the complex

We measure the H I flux of the complex in two ways: by measuring the total flux in a moment 0 map summed spectrally across the  $260$ – $790 \text{ km s}^{-1}$  velocity range in a  $37' \times 35'$  region centered on  $12^{\text{h}}30^{\text{m}}41^{\text{s}}$ ,  $09^{\circ}30'38''$  (fully enclosing points above  $3\sigma$  on the moment 0 map) and by measuring the total flux over the same velocity range in a spectrum summed spatially across the same region (these are shown in Figure 7). These are corrected using

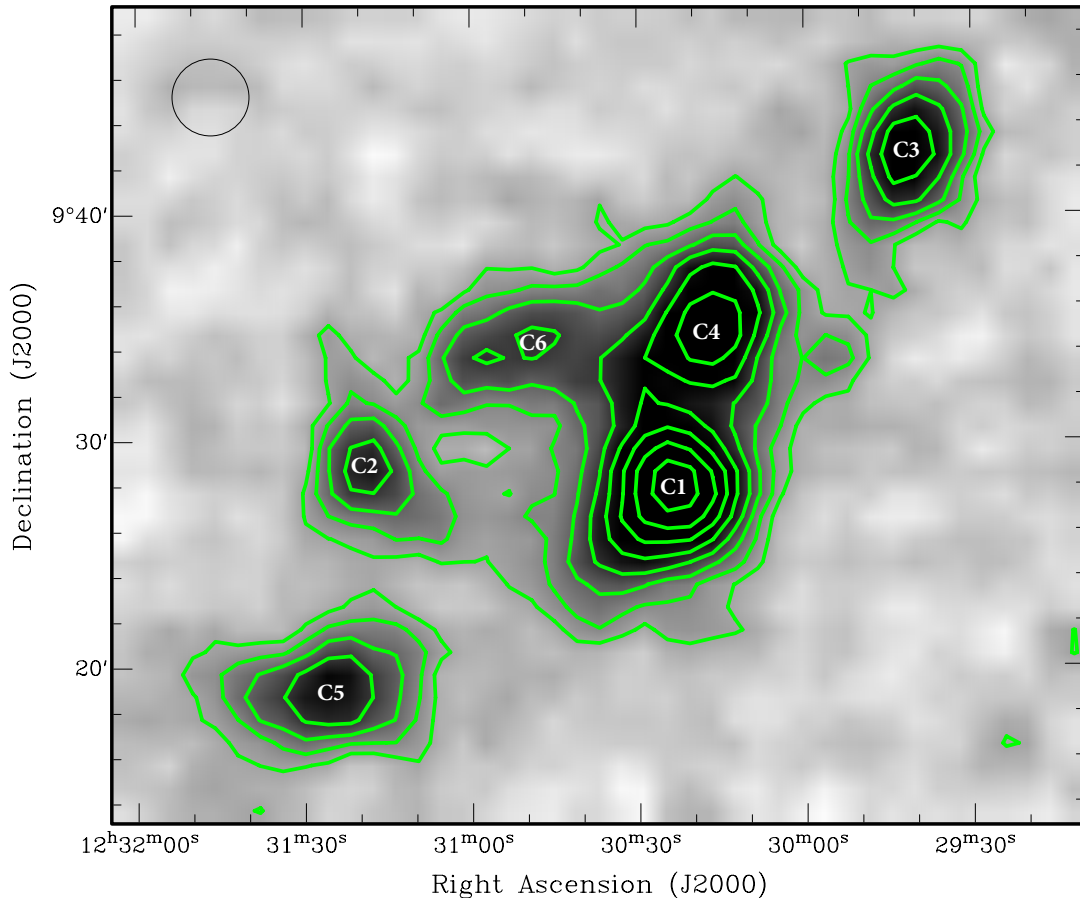


**Figure 2.** Moment 0 map over  $440$  to  $620$   $\text{km s}^{-1}$  with contours at  $0.18, 0.30, 0.45, 0.65, 0.90, 1.20, 1.55, 1.95$   $\text{Jy km s}^{-1}$  (equivalent to  $5, 8, 12, 18, 24, 32, 42, 53 \times 10^{19} \text{ cm}^{-2}$  for resolved structures), with clouds labeled. The velocity range is chosen to illustrate all 6 clouds at a good signal-to-noise and does not include all of the gas in the complex (see below). The Arecibo beam is shown by the black circle in the upper left corner.

a circular Gaussian beam of HPBW  $3.4'$ . The moment 0 map gives a total flux of  $26.6 \pm 1.3$   $\text{Jy km s}^{-1}$  and the spectrum gives a total flux of  $28.0 \pm 1.7$   $\text{Jy km s}^{-1}$ . While these are not significantly different, they are different enough that using a polygonal map to better fit the shape of the complex is unlikely to bring a major improvement in signal to noise while potentially missing some diffuse gas. Combining the measurements from the two methods gives a value of  $27.3 \pm 2.2$   $\text{Jy km s}^{-1}$ .

This total flux measurement needs to be adjusted for the sidelobes, which are not included in the Gaussian primary beam correction, and which contain significant flux scattered out of the main beam. As the first minimum occurs at  $\sim 3.7'$  from the beam center and the peak of the first sidelobe is at  $\sim 5.6'$ , for a measurement box size larger than  $5' \times 5'$  at least part of the first sidelobe will fall within the box and will thus lead to an overestimate of the flux if this is not corrected for (a sidelobe correction is not necessary for normal point-source measurements in AGES as these are made within a  $5' \times 5'$  box, falling entirely within the  $\sim 3.7'$

radius of the first minimum and thus not including any sidelobe flux). A box of size  $15' \times 15'$  or greater should fully enclose the first sidelobe, thus our map (which is substantially larger than this) will contain both main-beam flux and flux from the sidelobes, both of which will contribute to our measured flux. Heiles et al. (2001) found the ratio of the first sidelobe and main beam efficiencies to be  $\eta_{\text{FS}}/\eta_{\text{MB}} = 0.33$  for the LBW feed, while Heiles (2004) found values for the ALFA beams of  $\eta_{\text{FS}}/\eta_{\text{MB}} = 0.16$  for the central beam and varying from  $0.30$  to  $0.38$  for the outer beams. The average across all ALFA beams is  $\eta_{\text{FS}}/\eta_{\text{MB}} = 0.31$  and the median is  $0.33$ . We adopt a value of  $\eta_{\text{FS}}/\eta_{\text{MB}} = 0.33$  and correct our measured flux by a factor of  $1 + \eta_{\text{FS}}/\eta_{\text{MB}}$ , giving  $20.5 \pm 1.7$   $\text{Jy km s}^{-1}$ . This assumes no significant contribution from other sidelobes: as  $\langle \eta_{\text{MB}} + \eta_{\text{FS}} \rangle = 0.75$ , sidelobes beyond the first contain around 25 percent of the total flux, but the majority of this will be scattered well outside our map; we therefore follow Peek et al. (2011) in not attempting a correction for the more distant sidelobes.

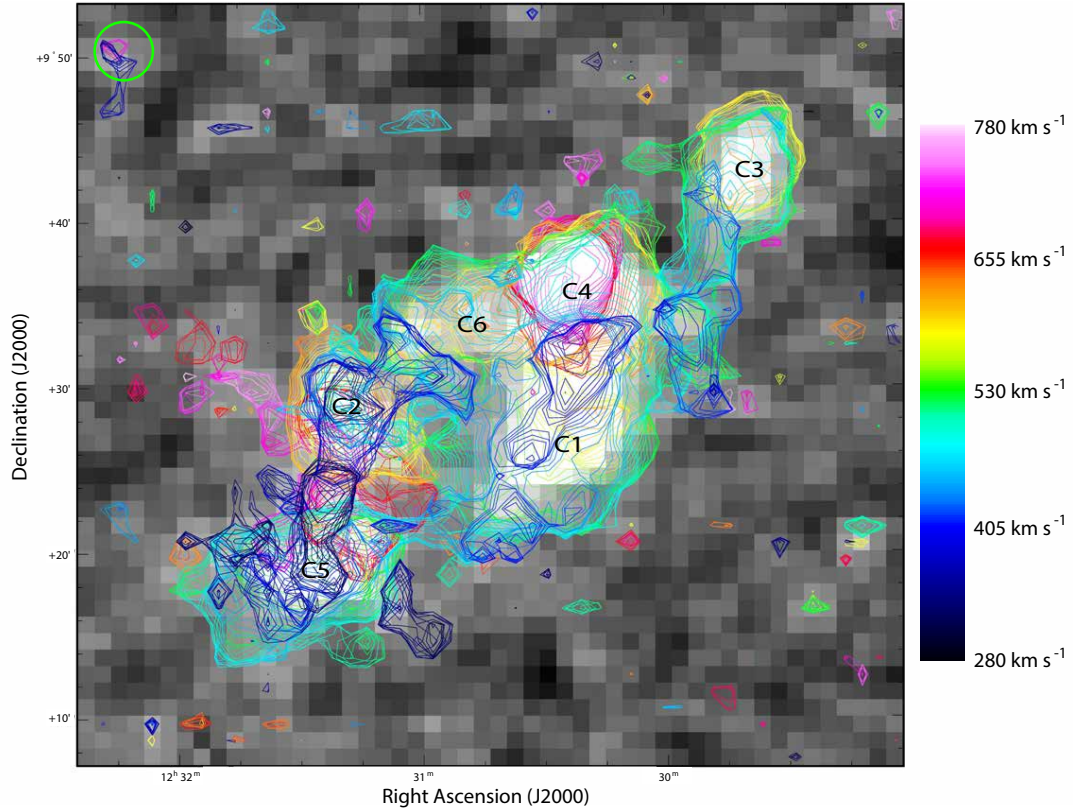


**Figure 3.** Renzogram of the cube boxcar smoothed in velocity over a width of 11 channels to a velocity resolution of  $55 \text{ km s}^{-1}$ . Contours are at  $1.5 \text{ mJy beam}^{-1}$  (equivalent to a column density of  $2.2 \times 10^{18} \text{ cm}^{-2}$  for resolved structures; note that this is much lower than the column densities in Figure 2 due to the lower velocity range covered by each contour). Colors indicate velocity, using a ‘Rainbow’ color map from  $280 \text{ km s}^{-1}$  (violet) to  $780 \text{ km s}^{-1}$  (red). A renzogram can be thought of as over-plotted color-coded channel maps, allowing the connections between structures at different velocities to be seen much more easily than with a traditional channel map and at a much higher resolution than would be possible with a large grid of traditional channel maps. Greyscale shows the moment 0 map over the velocity range  $250\text{--}800 \text{ km s}^{-1}$ . The green circle in the top left indicates the beam size.

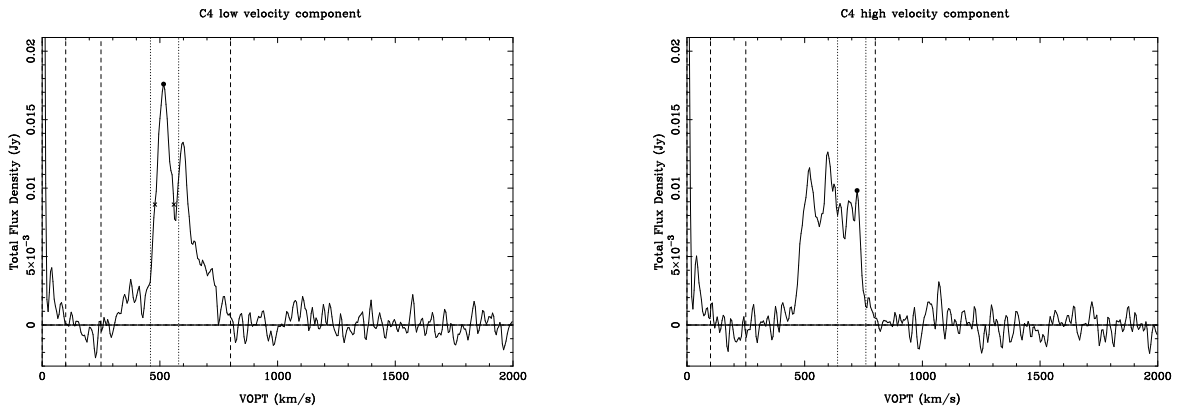


**Figure 4.** Spectra of the low velocity (left) and high velocity (right) components of C4, summed and beam-corrected over a  $5' \times 5'$  region. Dotted lines mark out the velocity range used for the position fit. A first order baseline has been subtracted from both spectra; the region over which this was fitted is indicated by the extent of the spectra dashed lines indicate the ranges excluded from the baseline fit (below  $100 \text{ km s}^{-1}$  to exclude Galactic hydrogen and  $250\text{--}800 \text{ km s}^{-1}$  to exclude the complex itself).

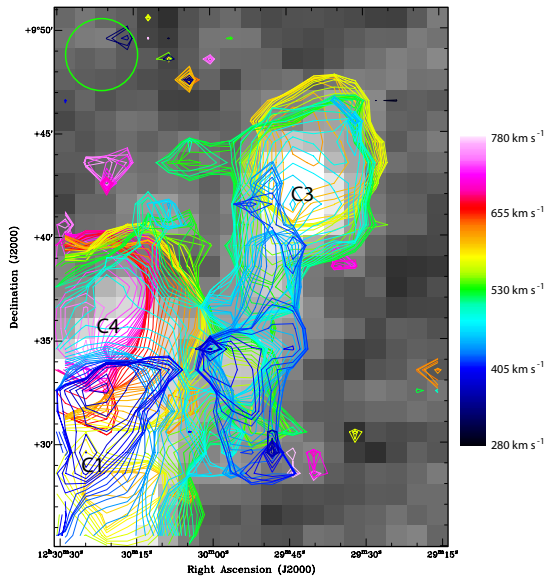


**Figure 5.** Zoomed region of the renzogram in Figure 3 showing the bridge between C3 and the main (C1-C4) complex. Greyscale shows a moment 0 map over  $400 - 520 \text{ km s}^{-1}$ . The green circle in the top left indicates the beam size.

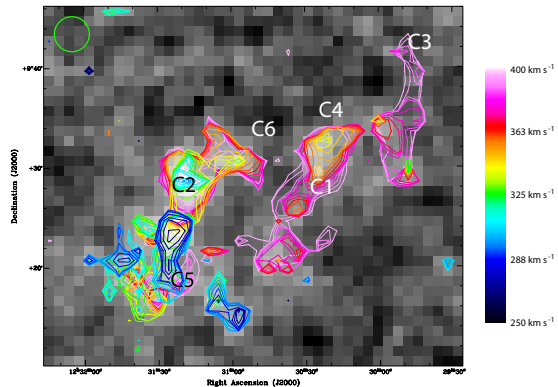


**Figure 6.** Renzogram (rainbow colormap; contour levels as in Figure 3) and moment 0 map (greyscale) of low velocity gas over  $250-400 \text{ km s}^{-1}$ . The green circle in the top left indicates the beam size.

We therefore measure a total HI mass of  $1.3 \pm 0.1 \times 10^9 M_{\odot}$ , assuming the same distance of 16.7 Mpc used by Kent et al. (2009). This is considerably higher than their total HI mass measurement of  $5.1 \times 10^8 M_{\odot}$ . However, their total flux is simply the sum of the flux found in each cloud, to which we have added substantial extended emission and emission from smaller clouds that could explain the discrepancy. To check this, we compare the measurements from single-point spectra at the locations Kent et al. (2009) identify as the cloud centers. For consistency, the errors for Kent et al. (2009) were recalculated using the formulae of Koribalski et al. (2004) and the quoted S/N.

We find that our measurements of the individual clouds are consistent with Kent et al. (2007, 2009). There are no significant differences in fluxes on individual clouds between the WAVES single-point spectra and the Kent et al. (2009) measurements, and summed across the five clouds identified by Kent et al. (2009) we see less emission than they do, although not significantly ( $7.20 \pm 0.30$  vs  $7.83 \pm 0.92 \text{ Jy km s}^{-1}$ ; errors following Koribalski et al. (2004)). Thus the extra flux seen in our map would appear to be from extended emission and newly identified clouds not included in the total by Kent et al. (2009). The only significant difference between our measurements and Kent et al. (2009) is on the central velocity and velocity width of cloud C3. This inconsistency can be traced to a narrow secondary peak near  $600 \text{ km s}^{-1}$  that is above 50 percent of the flux of the primary peak in the Kent et al. (2009) spectrum, thus increasing their 50 percent velocity width and shifting their velocity center, but which falls below 50 percent of the peak of the primary in the corresponding single-point WAVES spectrum (the peak in question can be seen in our spatially-integrated spectrum of C3 in Figure 8, where it is again above 50 percent).

### 3.2. HI parameters of individual clouds

Measuring over a  $5' \times 5'$  box allows us to fit positions for the clouds in addition to measuring their parameters (Table 1). In addition to the 5 clouds found by Kent et al. (2007, 2009), we also fit for cloud C6 and the new low-velocity components of clouds C2 and C5, here labeled C2b and C5b, which are separated kinematically from the clouds found by Kent et al. (2009). Although cloud C4 has two distinct center positions these are not clearly separated kinematically; thus we only make a single measurement of the flux, velocity width, etc. for that cloud. The spectra associated with these measurements are given in Figure 8.

The gas clouds identified in Table 1 contribute a total flux of  $11.2 \pm 0.4 \text{ Jy km s}^{-1}$ , compared with our measurement of  $20.5 \pm 1.7 \text{ Jy km s}^{-1}$  for the complex as a whole. Diffuse gas in between the compact clouds would thus appear to be responsible for at least  $45 \pm 4$  percent of the total gas in the complex, with the strong possibility that more exists below our detection threshold. Unlike in the single-point spectra discussed above, the fluxes in these spatially-extended spectra are higher than those found by Kent et al. (2009) for the same clouds, indicating the likely presence of extended flux around these sources.

## 4. NGC 4522

NGC 4522 is a classic example (see Figure 9) of a galaxy that is undergoing ram-pressure stripping, giving

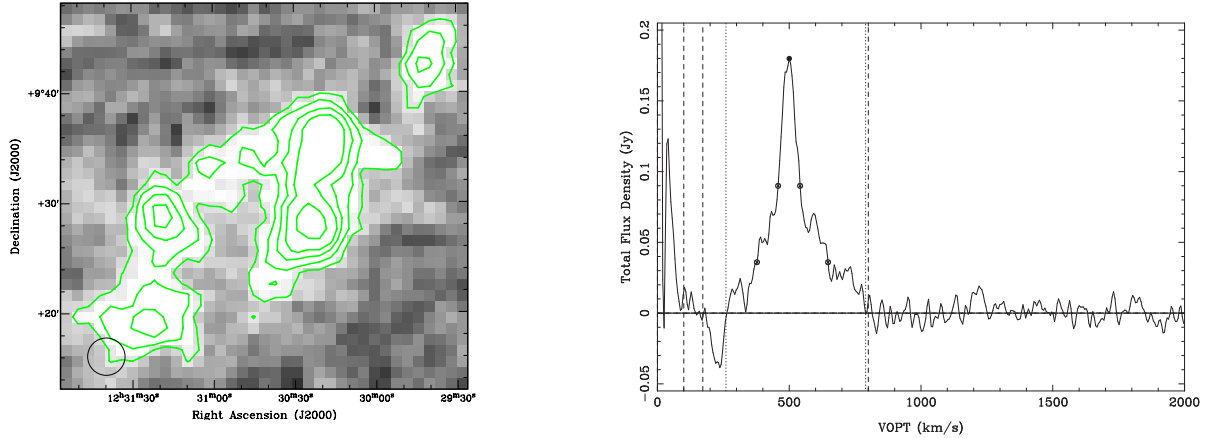


**Figure 7.** Left: Moment 0 map over 260 to 790  $\text{km s}^{-1}$  of the complex over the  $37' \times 35'$  region centered on  $12^{\text{h}}30^{\text{m}}41^{\text{s}}$ ,  $09^{\circ}30'38''$  used for total flux measurements, with contours showing  $3\sigma$ ,  $5\sigma$ ,  $7.5\sigma$ ,  $10\sigma$ ,  $15\sigma$  (over the full velocity width, so narrow features such as the bridge between C1/C4 and C3 are washed out by noise from other channels). Right: Spectrum over the same area showing the measurement range (dotted line). A first order baseline has been subtracted from the spectrum; the region over which this was fitted is indicated by the extent of the spectrum; dashed lines indicate the ranges excluded from the baseline fit (below  $100 \text{ km s}^{-1}$  to exclude Galactic hydrogen and  $180\text{--}800 \text{ km s}^{-1}$  to exclude the complex itself and the nearby negative feature); the negative feature at  $180$  to  $260 \text{ km s}^{-1}$  is an artefact from high velocity Galactic hydrogen in the eastern part of the cube.

**Table 1.** Measurements of the clouds in a  $5' \times 5'$  box. Errors calculated using the formulae of [Koribalski et al. \(2004\)](#).

ID	RA (J2000)	Decl. (J2000)	$V_{50}$ ( $\text{km s}^{-1}$ )	$W_{50}$ ( $\text{km s}^{-1}$ )	$W_{20}$ ( $\text{km s}^{-1}$ )	$F_{\text{HI}}$ ( $\text{Jy km s}^{-1}$ )	$M_{\text{HI}}$ ( $10^8 M_{\odot}$ )	$S_{\text{peak}}$ (mJy)	Peak SNR
C1	12:30:24.6	09:27:59	$496 \pm 2$	$70 \pm 5$	$113 \pm 7$	$3.06 \pm 0.22$	$2.01 \pm 0.14$	35	67
C2	12:31:19.2	09:28:40	$607 \pm 3$	$57 \pm 7$	$108 \pm 10$	$0.94 \pm 0.10$	$0.62 \pm 0.06$	14	18
C2b	12:31:19.9	09:28:59	$386 \pm 7$	$127 \pm 14$	$192 \pm 21$	$0.57 \pm 0.09$	$0.37 \pm 0.06$	6	8.0
C3	12:29:42.2	09:42:39	$538 \pm 2$	$121 \pm 4$	$148 \pm 7$	$1.40 \pm 0.12$	$0.91 \pm 0.08$	15	23
C4	12:30:19.9	09:35:47	$566 \pm 4$	$172 \pm 8$	$278 \pm 12$	$2.73 \pm 0.16$	$1.79 \pm 0.11$	16	29
C5	12:31:25.8	09:18:49	$486 \pm 4$	$63 \pm 8$	$144 \pm 11$	$1.27 \pm 0.11$	$0.83 \pm 0.07$	16	27
C5b	12:31:28.7	09:18:29	$307 \pm 8$	$57 \pm 15$	$107 \pm 23$	$0.28 \pm 0.07$	$0.18 \pm 0.05$	4	6.7
C6	12:30:47.3	09:34:04	$538 \pm 5$	$115 \pm 11$	$164 \pm 16$	$0.97 \pm 0.13$	$0.64 \pm 0.09$	9	11

rise to an optically-dark HI tail of gas removed from the galaxy. VLA HI observations by [Kenney et al. \(2004\)](#) and [Chung et al. \(2007\)](#) show a tail of around 40 arcsec in length beyond the plane of the galaxy; [Kenney et al. \(2004\)](#) further derive an HI deficiency of 0.6, indicating that around three quarters of the original gas content has been lost from this galaxy. [Vollmer et al. \(2006\)](#) successfully simulate the extra-planar HI and the HI deficiency by assuming the galaxy is traveling at a high speed ( $\sim 3500 \text{ km s}^{-1}$ ) relative to the ICM, either because it is not bound to the cluster or because the ICM is itself moving with respect to the cluster due to the infall of the M49 group. In their simulations, the

galaxy has an initial gas mass of  $1.3 \times 10^9 M_{\odot}$ , of which  $9 \times 10^8 M_{\odot}$  is lost.

To this, our new observations add the discovery of a high velocity (relative to the galaxy) extension of the gas tail of NGC 4522. This stretches about  $200 \text{ km s}^{-1}$  below the velocity of the HI seen in the galaxy, to a recessional velocity of  $2000 \text{ km s}^{-1}$ , and has a slight inclination seen in a velocity-RA map (Figure 10), shifting around 25 seconds in RA ( $6' = 30 \text{ kpc}$  at a distance of  $16.7 \text{ Mpc}$ ) west along its length to  $13:33:15$ . The [Vollmer et al. \(2006\)](#) simulations reproduced the blueshift of the HI velocities in the tail relative to the galaxy seen in the VLA observations of [Kenney et al. \(2004\)](#), but not the velocity width seen there of  $150 \text{ km s}^{-1}$  (full width at

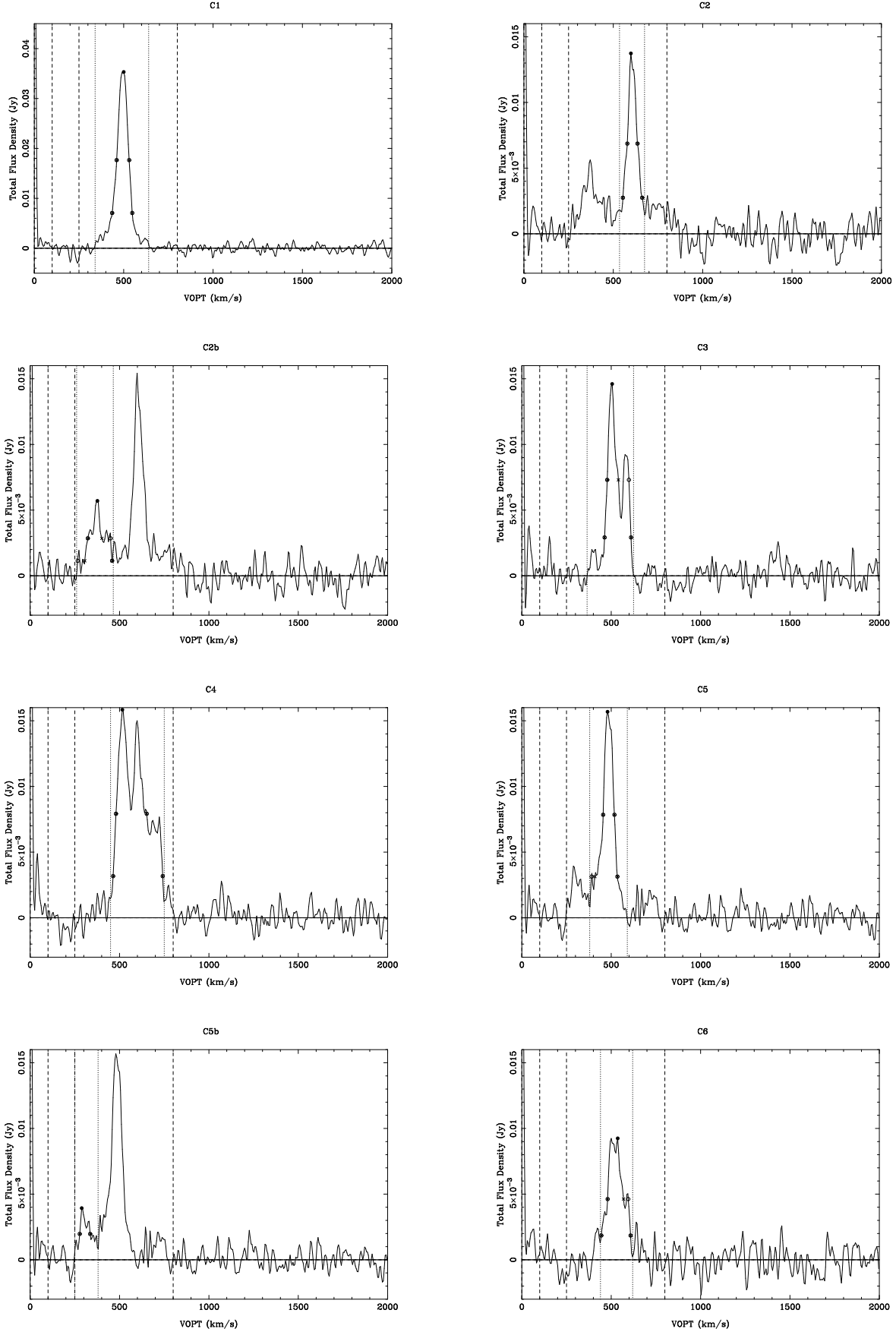


**Figure 8.** Spectra of the clouds used for the measurements in Table 2. Left to right, top row: C1, C2; second row: C2b, C3; third row: C4, C5; bottom row: C5b, C6. For all spectra, dotted lines indicate the velocity range used to derive the parameters given in Table 1. The region used for the baseline fit is indicated by the extent of the spectra; dashed lines indicate velocity ranges excluded from the fit due to possible contamination from the complex or Galactic gas.



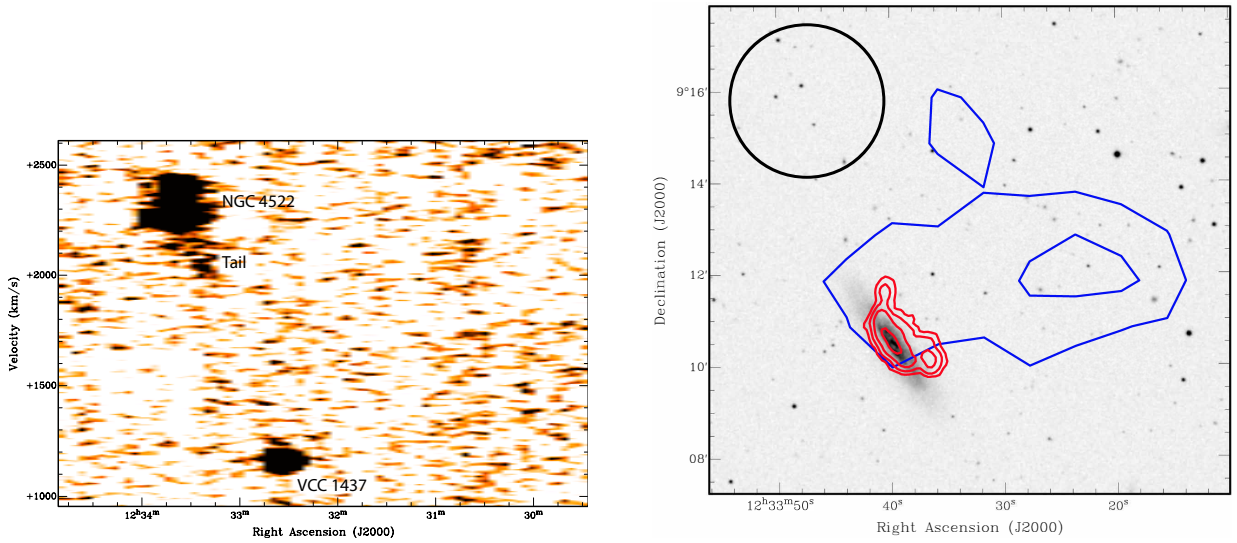


**Figure 9.** Left: Position-velocity map showing velocity as a function of RA, covering the declination range  $09^{\circ}11'$  to  $09^{\circ}13'$  (the range over which the tail is visible in the data cube), showing the tail to low velocities on NGC 4522 and the galaxy VCC 1437. Right: Gray scale shows the DSS image of the galaxy with blue contours showing the WAVES moment 0 map covering 2000 to  $2200 \text{ km s}^{-1}$  in velocity (i.e. only velocities below those of the main body of the galaxy) at  $5 \times 10^{18} \text{ cm}^{-2}$  and  $1 \times 10^{19} \text{ cm}^{-2}$ , illustrating the eastwards extension of the tail from NGC 4522, and red contours showing the VLA moment 0 map from VIVA (Chung et al. 2007), covering around  $2170$  to  $2470 \text{ km s}^{-1}$ , at  $2 \times 10^{20}$ ,  $5 \times 10^{20}$ ,  $1 \times 10^{21}$  and  $2 \times 10^{21} \text{ cm}^{-2}$ . The Arecibo beam is shown to the top left.

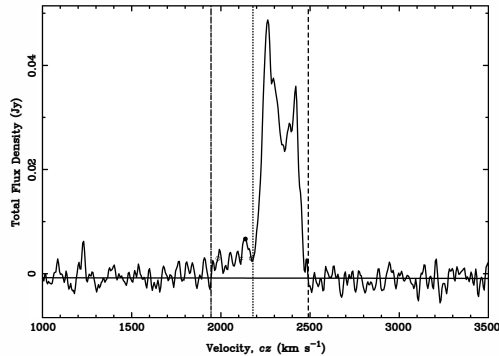


**Figure 10.** Spectrum of NGC 4522 summed over a  $13' \times 7'$  box centered on  $12^{\text{h}}33^{\text{m}}30^{\text{s}}$ ,  $09^{\circ}12'00''$  and primary beam corrected. A first order (linear) baseline has been fitted and is shown; the extent of the spectrum indicates the region over which this fit was made. Dashed lines at 1945 and 2490  $\text{km s}^{-1}$  indicate the area masked from the baseline fit and dotted lines at 1945 and 2180  $\text{km s}^{-1}$  indicate the area used for the measurement of the tail.

zero intensity). Our addition of an extra  $200 \text{ km s}^{-1}$  to this is thus well out of the range of gas dynamics reproduced by the simulations. The direction of the tail we observe is consistent with the angle of  $-15 \text{ deg}$  (north of west) assumed by Vollmer et al. (2006) based on HST observations.

The extension of the tail can be seen in the spectrum of NGC 4522 as a faint wing on the low velocity side of the main peak (Figure 10). From measurements on the spectrum, summed over a  $13' \times 7'$  box centered on  $12^{\text{h}}33^{\text{m}}30^{\text{s}}$ ,  $09^{\circ}12'00''$ , the wing has an HI flux of  $0.9 \pm 0.2 \text{ Jy km s}^{-1}$  within a velocity range from the minimum between the galaxy and the tail at  $2180 \text{ km s}^{-1}$  to when it falls to zero intensity at  $1945 \text{ km s}^{-1}$ . This gives an HI mass (at 16.7 Mpc) of  $5.9 \pm 1.3 \times 10^7 M_{\odot}$ . By comparison we measure (on the same spectrum) a flux of  $7.9 \pm 0.5 \text{ Jy km s}^{-1}$  for the galaxy between the minimum at  $2180 \text{ km s}^{-1}$  and when it falls to zero intensity at  $2490 \text{ km s}^{-1}$  equivalent to  $5.2 \times 10^8 M_{\odot}$  (due to the size of the box, this will include a small contribution from the sidelobes). Measurement assuming a point source at the position of the HI peak of the galaxy gives a flux of  $6.4 \pm 0.3 \text{ Jy km s}^{-1}$ , equivalent to  $4.2 \times 10^8 M_{\odot}$ . These are both consistent with the  $7 \pm \sim 1 \text{ Jy km s}^{-1}$  measured in a single Arecibo pointing by Helou, Hoffman & Salpeter (1984), and bracket the  $7.17 \pm 0.10 \text{ Jy km s}^{-1}$  measured by ALFALFA (Haynes et al. 2018).

Allowing for beam smearing, the WAVES tail extends around  $5'$  from the galaxy to a column density of  $\sim 10^{19} \text{ cm}^{-2}$ . This is  $\sim 7.5$  times longer than the tail visible on the VIVA maps from the VLA (Chung et al. 2007),

over which distance the column-density falls by a factor of  $\sim 20$ . The tail density therefore decreases approximately as  $N_{\text{HI}} \propto d^{-1.5}$ . This is consistent with geometrical dilution being the dominant process in making the tail invisible, as inferred from comparison with results of Roediger & Brügger (2007) and from computations of test particle models as in Köppen et al. (2018).

## 5. DISCUSSION – POSSIBLE ORIGINS OF THE ALFALFA VIRGO 7 COMPLEX

Kent et al. (2009) propose that a possible scenario for the origin of the ALFALFA Virgo 7 complex is stripping from a galaxy, with the nearby galaxies NGC 4445 and NGC 4424 (both at similar redshifts to the complex) being identified as possible candidates for the parent galaxy. Our results above, showing an alignment both spatially and in velocity-space between the complex and the tail of NGC 4522, mean that we must also consider the possibility that this galaxy is associated with the complex. In Figure 11 we show the region around the complex, with the nearby galaxies labelled and color-coded by redshift, and with HI contours shown for those detected in WAVES.

An approximate separation/dispersion timescale for the complex can be calculated from the velocity differences between the clouds,  $\Delta V$ , and their projected separation,  $r$ , i.e.  $\tau \sim r/\Delta V$ , assuming a common starting point. It can be seen from Table 2 that a timescale of around 1 Gyr is consistent with the current dispersion of the clumps in the cloud. It can also be seen that if, alternatively, the complex is a bound system (which seems highly unlikely) it would have a dynamical mass of approximately  $10^{11} - 10^{12} M_{\odot}$ .

The ALFALFA Virgo 7 complex is similar in some ways to the cloud HI 1225+01 in the Virgo southern extension (Giovanelli & Haynes 1989; Giovanelli, Williams & Haynes 1991). At their assumed distance of 20 Mpc, HI 1225+01 has a total mass of  $4.9 \times 10^9 M_{\odot}$  with the two clumps to the NE and SW of the cloud having masses of  $2.4 \times 10^9 M_{\odot}$  and  $1.3 \times 10^9 M_{\odot}$  respectively (Giovanelli, Williams & Haynes 1991). Approximately a third of the emission is from diffuse gas rather than from the two clumps. This combination of multiple HI clouds and diffuse emission is reminiscent of the complex here, but there are important differences. The more massive NE clump of HI 1225+01 hosts a low surface brightness dwarf irregular galaxy, J1227+0136 (Djorgovski 1990; Impey et al. 1990; McMahan et al. 1990), although no counterpart has been found to the SW clump despite repeated searches down to  $27-28 \text{ mag arcsec}^{-2}$  (Impey et al. 1990; Salzer et al. 1991; Turner & MacFayden 1997; Matsuoka et al. 2012). Chengalur, Giovanelli & Haynes

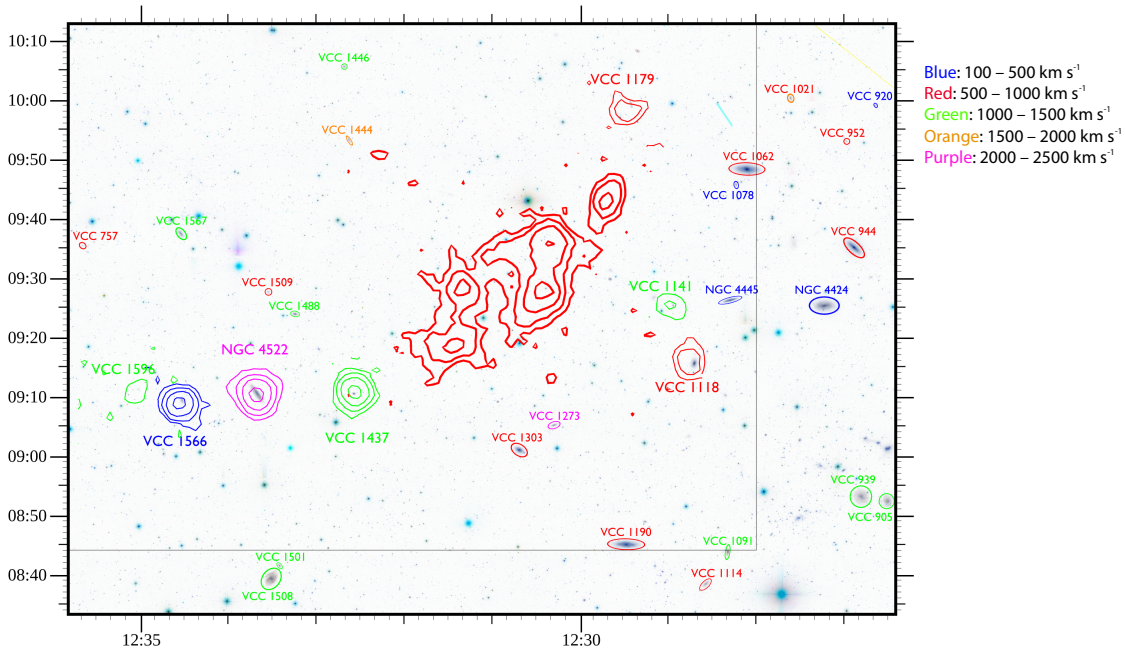


**Figure 11.** Significant galaxies near the ALFALFA Virgo 7 complex. H I contours from WAVES are shown for those galaxies detected (contour levels vary between sources due to their different fluxes and velocity widths and are set to ensure the individual sources are visible); others (undetected or outside of the current WAVES coverage) are shown by ellipses. Contours and ellipses are color-coded by velocity. Thin gray lines show the boundaries of the WAVES coverage.

**Table 2.** Timescales for the clouds to have reached their current separation from the central C1 cloud and implied dynamical mass of the complex (assuming  $\delta V = V_{\text{circ}}$ ) if it were bound.

Cloud	Velocity difference from C1 (km/s)	Projected distance from C1 (kpc)	Timescale (Gyr)	Implied dynamical mass ( $10^{10} M_{\odot}$ ).
C2	$111 \pm 4$	67	0.6	19
C2b	$110 \pm 7$	68	0.6	19
C3	$42 \pm 3$	88	2.0	3.6
C4	$70 \pm 4$	38	0.5	4.3
C5	$10 \pm 4$	87	8.5	0.2
C5b	$189 \pm 8$	91	0.5	76
C6	$42 \pm 5$	41	1.0	17

(1995) suggested that the SW clump could be an edge-on disc; it has also been suggested (Turner & MacFayden 1997) that it could be a tidal tail from the NE clump although this has not been the subject of detailed modeling.

### 5.1. NGC 4445 and NGC 4424

These two galaxies were suggested by Kent et al. (2009) as possible parent galaxies, but the discovery

of much more neutral hydrogen in the complex affects the likelihood of this. They have estimated original H I masses based on their optical diameters and morphological types (Solanes, Giovanelli & Haynes 1996) of  $1.2^{+0.9}_{-0.6} \times 10^9 M_{\odot}$  and  $1.7^{+1.4}_{-0.8} \times 10^9 M_{\odot}$  respectively, at our adopted distance for the complex of 16.7 Mpc. We measure an H I mass for the complex of  $1.3 \pm 0.1 \times 10^9 M_{\odot}$ . Sorgho et al. (2017), using a combined WSRT and KAT-7 map, measure current H I masses for these galax-

ies, corrected to our adopted distance, of  $0.3 \pm 0.1 \times 10^8 M_{\odot}$  and  $2.4 \pm 0.5 \times 10^8 M_{\odot}$ . This means they have lost  $1.2^{+0.9}_{-0.6} \times 10^9 M_{\odot}$  and  $1.5^{+1.4}_{-0.8} \times 10^9 M_{\odot}$  respectively. The gas detected in the complex would thus account for 110 percent of the expected gas lost from NGC 4445 or 85 percent of the expected gas lost from NGC 4424. Even taking the upper ends of these distributions, the gas detected in the complex would account for over 60 percent of the gas lost from NGC 4445 and over 45 percent of the gas lost from NGC 4424. By comparison, most previously known HI streams in Virgo account for 20 percent or less of the expected (not upper end) mass lost from their parent galaxies (Taylor et al. 2019, submitted), while the new streams identified in that paper generally contain less than 10 percent of the mass lost from their parents. The ALFALFA Virgo 7 complex would thus, if it originated in either of these galaxies, contain a uniquely high fraction of the missing gas from its progenitor galaxy for any dark feature.

Of the two, the more obvious candidate is NGC 4445: it has lost virtually all of its original gas mass and it is close by and at a similar velocity to the complex. As the ram pressure necessary to account for the deficiency of NGC 4445 is higher than the pressure estimated at its present location, it is likely to have had its stripping in the past (Köppen et al. 2018). However, as mentioned above, even if it were unusually gas rich the HI mass we measure in the complex would account for over 60 percent of the gas lost from this galaxy. Evaporation for a free-floating cloud is expected to be at a rate of  $1 - 10 M_{\odot}$  per year, or around  $10^9 - 10^{10} M_{\odot}$  over the approximately 1 Gyr timescale of the cloud (Taylor et al. 2019, submitted), so this accounts for the rest of the gas lost. If NGC 4445 is the parent galaxy of the complex, this implies that we have now discovered virtually all of the gas to be found and that it has been removed from the galaxy remarkably efficiently, with little gas dispersed to low column densities. NGC 4445 has a short tail pointing away from the complex (Sorgho et al. 2017) and is not well aligned with the complex, although if the stripping occurred near a pericentric passage and both objects have moved and separated since then this is not a strong objection.

NGC 4424 lies close to NGC 4445 both spatially and in velocity. The amount of gas lost from this galaxy is more consistent with the gas seen in the complex, but it is known to be currently losing gas via ram-pressure stripping, with a long HI tail to the south-east (Chung et al. 2007; Sorgho et al. 2017). This creates not only an alignment problem – the tail points nowhere near the complex – but also the problem that creating the complex as a structure separate from the current tail would

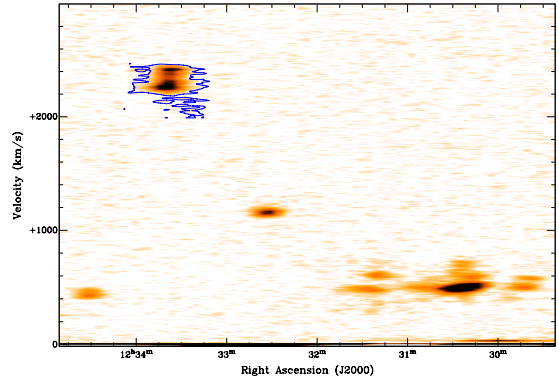


**Figure 12.** Moment 0 map in RA against velocity covering the whole region and clipped at  $3\sigma$ . The tail on NGC 4522 is shown by the blue contours (from the position-velocity plot shown in Figure 10, at a flux summed in declination of 5 mJy). The alignment between NGC 4522 and its tail, VCC 1437, and the eastern end of the complex can be easily seen. VCC 1566 is also visible at the east side of the plot.

require two discrete stripping episodes. It is hard to envision a scenario in which this could occur, without requiring significant, unexpected sub-structure in Virgo’s ICM.

## 5.2. NGC 4522

Could there be a connection between the ALFALFA Virgo 7 complex and NGC 4522? It can be seen from Figures 11 and 12 that there is an intriguing alignment on the sky between NGC 4522, VCC 1437 and the complex, similar to that expected if the complex were deposited as a stream by NGC 4522. Figure 13 shows that there is also an alignment in velocity space between the current tail and the eastern end of the complex (and VCC 1437), making it very tempting to interpret these as being connected. Based on NGC 4522’s optical radius (SDSS, isophotal) of 120 arcsec and its Sc morphology it is expected to have had (following Solanes, Giovanelli & Haynes 1996) an initial mass of  $2.5^{+1.5}_{-0.9} \times 10^9 M_{\odot}$ , while our measurement of  $7.9 \pm 0.5 \text{ Jy km s}^{-1}$  gives an HI mass (at 16.7 Mpc) of  $5.2 \pm 0.3 \times 10^8 M_{\odot}$ , for a loss of  $1.5^{+1.5}_{-0.9} \times 10^9 M_{\odot}$ , which is consistent with the HI mass needed to form the complex and gives a deficiency of  $0.7 \pm 0.2$ .

However, NGC 4522’s recessional velocity of  $2330 \text{ km s}^{-1}$ , over  $1800 \text{ km s}^{-1}$  higher than the complex, throws up two challenges: Firstly, the extreme velocity difference between the complex and the galaxy makes any connection between the two appear unlikely (Kent et al. 2009 do not consider NGC 4522 except to note that it is close in projection but in a different velocity regime). Secondly, the distance from C3 to NGC 4522 is  $68'$ , while the distance from C5 is  $35'$ . If the complex

had been lain down as NGC 4522 moved through the cluster, we might expect the velocity C5 to lie about half way between that of C3 and NGC 4522, i.e. about  $900 \text{ km s}^{-1}$  higher. But C5 actually lies at a velocity  $52 \pm 4 \text{ km s}^{-1}$  lower than that of C3.

Although NGC 4522 lies at a significantly different velocity, it has already been posited (Kenney et al. 2004; Vollmer et al. 2004, 2006) to be moving at a high velocity ( $3500\text{--}4000 \text{ km s}^{-1}$ ) relative to the local ICM, either because it is not bound to the cluster or because the ICM itself is in motion due to the infall of the M49 group. The tail to lower velocities revealed by our observations indicates that it is certainly moving at a significantly higher recessional velocity than its local ICM. Gas removed from NGC 4522 would be expected to eventually come to rest at the velocity of the ICM, which could potentially explain the relatively flat velocity profile of the complex and its separation in velocity space from NGC 4522.

The simulations of Vollmer et al. (2006) find a best fit for an inclination of the galactic disc to the ICM wind of  $60^\circ$ , which gives a maximum line-of-sight component of the ICM wind of around 0.33. For the local ICM to be at the  $500 \text{ km s}^{-1}$  velocity of the complex would require this component to be around 0.46 for the highest relative velocity considered ( $4000 \text{ km s}^{-1}$ ). This would be possible for their  $45^\circ$  inclination simulation, which has a maximum line-of-sight component of around 0.56, but this simulation does not reproduce the observed extraplanar gas. It thus seems unlikely that the local ICM line-of-sight velocity in the region could be low enough to explain the complex as coming from NGC 4522.

In addition to this, and similarly to NGC 4424, NGC 4522 is currently being stripped and would thus also require two discrete stripping episodes. Putting all of these together, it seems unlikely that NGC 4522 is the parent galaxy for the complex.

### 5.3. Interactions

An alternative mechanism to ram-pressure stripping for removing gas from galaxies is tidal interactions, which are thought to be responsible for some of the other dark clouds identified in the Virgo cluster. For example, the VIRGOHI 21 cloud, which is most likely to have been caused by a fairly extreme hyperbolic interaction (Bekki, Koribalski & Kilborn 2005; Duc & Bournaud 2008; Taylor et al. 2017), has a mass of  $2.2 \times 10^8 M_\odot$  (Minchin et al. 2005) with a total mass of the cloud and the stream connecting it to NGC 4254 of  $4.3 \times 10^8 M_\odot$  (Haynes, Giovanelli & Kent 2007). NGC 4254 itself, meanwhile, has an H I mass of  $4.3 \times 10^9 M_\odot$  (Giovanelli et al. 2007). The event that created VIRGOHI 21 would

thus appear to have removed around 5 percent of the mass of the parent galaxy into the compact cloud and a further 5 percent into the stream. Simulations by Taylor et al. (2017) show that, in multiple runs, the parent galaxy typically retains 90–95 percent of its original gas content.

However, unlike ram pressure stripping which only affects the gas in a galaxy, tidal interactions have, in principle, equally strong effects on gas and stars. In practice, the gas disks of galaxies are usually very different from the stellar disks: the gas tends to be more extended than the stars but its density drops exponentially beyond the edge of the stellar disk (e.g. Bigiel & Blitz 2012; Broeils & Rhee 1997). This means that tidal encounters can disrupt the outermost gas without much affecting the stars, but since the density of this outer gas is low, such disruptions cannot remove significant amounts of gas. The only way for a tidal encounter to remove a high fraction of a galaxy’s gas content is if it is also strong enough to affect the inner, denser regions, which would necessarily also disrupt the stellar disk. Bekki, Koribalski & Kilborn (2005), for example, found that in their simulations (with a model galaxy which followed Broeils & van Woerden 1994, in having a gas disk twice the size of the stellar disk) the mass fraction of stars within their isolated clouds was 14 to 57 percent. Similarly, Taylor et al. (2017) found that “there is not so much difference in the typical fraction of gas and stars that are stripped”, with median fractions remaining in the disk of the parent galaxy of 92 percent for the gas and 95 percent for the stars. It does not seem likely that a tidal interaction with another galaxy could remove most of the gas in a galaxy while leaving that galaxy intact optically, thus a galaxy the size of NGC 4445 or NGC 4424 could not be the parent galaxy in a tidal interaction scenario.

A more plausible alternative, in the abstract, might be to scale up the parent galaxy by an order of magnitude so the removal of  $2 - 3 \times 10^9 M_\odot$  or more is only a relatively small percentage of the total H I mass. This would, however, require a parent galaxy with a few times  $10^{10} M_\odot$  of H I originally (90–95 percent of which would be retained; Taylor et al. 2017), and a similarly massive interactor to pull the gas out – such galaxies do exist but are rare, and there are no candidates in this part of the Virgo cluster. We would expect that, as with VIRGOHI 21 and the simulations it inspired, at least the parent galaxy would still be relatively nearby, even if a hyperbolic interactor was now too distant to be identified. It thus seems unlikely that interactions can provide a plausible mechanism for the creation of the complex.

## 6. CONCLUSIONS

NGC 4522 can be ruled out as a likely source galaxy for the ALFALFA Virgo 7 complex. The galaxy, with its tail pointing towards the eastern end of the complex both spatially and in velocity, is the only large nearby galaxy with any hint of a connection to the complex, but its large velocity separation makes this association dubious at best. Earlier simulations (by Vollmer et al. 2006) that might have allowed the gas in the complex to have come to rest with respect to the local ICM do not successfully reproduce the extra-planar gas seen in this galaxy, and their simulations that do reproduce that gas place the recessional velocity of the local ICM near NGC 4522 significantly higher than that of the complex.

NGC 4445 is a possible source galaxy for the complex, while NGC 4424 is a less likely candidate. Our sensitive 21-cm map of the complex reveals a large reservoir of gas that was not detected by ALFALFA. This gas is found in low velocity clouds associated with Kent et al. (2009)s C2 and C5 clouds, in a sixth cloud, termed C6, joined to the main body of the complex, and as low column-density gas between the clouds. Its detection raises the HI mass of the complex from  $0.5 \times 10^9 M_{\odot}$  to  $1.3 \times 10^9 M_{\odot}$ ; this counts against either NGC 4445 or NGC 4424 being a likely source galaxy for the complex. It is notable that NGC 4424 is currently being stripped, while NGC 4445 has lost much of its gas at some point in the past but is not currently thought to be undergoing stripping; It is possible that a single event in the past could have been responsible for this gas loss, from NGC 4445, potentially giving rise to the complex.

For the HI 1225+01 complex, Matsuoka et al. (2012) conclude that its formation process is still not well un-

derstood. We must similarly conclude that the origin of the complex remains without a satisfactory solution – none of the obvious mechanisms normally invoked can explain the presence of an isolated  $\sim 10^9 M_{\odot}$  neutral hydrogen complex in this location in the Virgo cluster. Our WAVES observations will cover the regions to the north and west of the complex over the next couple of years, which will allow us to identify any other gas clouds that might be associated with this complex and potentially give further clues towards its formation. As it stands, the least-worst candidate for the source galaxy remains NGC 4445, but this appears to require it to have been unusually gas-rich prior to the formation of the complex.

The Arecibo Observatory was operated at the time of these observation by SRI International under a cooperative agreement with the National Science Foundation (AST-1100968), and in alliance with Ana G. Méndez-Universidad Metropolitana, and the Universities Space Research Association. The SOFIA Science Center is operated by the Universities Space Research Association under NASA contract NNA17BF53C. R. Taylor was supported by the Czech Academy of Sciences GAČR grant CSF 19-18647S. We thank the anonymous referee for comments that have improved this paper.

*Facility:* Arecibo Observatory (ALFA)

*Software:* Karma (Gooch 1996), MIRIAD (Sault et al. 1995)

## REFERENCES

- Arrigoni Battaia, F., Gavazzi, G., Fumagalli, M., et al. 2012, A&A, 543, A112.
- Auld, R., Minchin, R. F., Davies, J. I., et al. 2006, MNRAS, 371, 1617.
- Bekki, K., Koribalski, B. S., & Kilborn, V. A. 2005, MNRAS, 363, L21
- Bigiel, F., & Blitz, L. 2012, ApJ, 756, 183
- Broeils, A. H., & Rhee, M.-H. 1997, A&A, 324, 877
- Broeils, A. H., & van Woerden, H. 1994, A&AS, 107, 129
- Chengalur, J. N., Giovanelli, R., & Haynes, M. P. 1995, AJ, 109, 2415.
- Chung, A., van Gorkom, J. H., Kenney, J. D. P., et al. 2007, ApJ, 659, L115.
- Davies, J., Minchin, R., Sabatini, S., et al. 2004, MNRAS, 349, 922.
- Djorgovski, S. 1990, AJ, 99, 31.
- Duc, P.-A., & Bournaud, F. 2008, ApJ, 673, 787.
- Giovanelli, R., & Haynes, M. P. 1989, ApJ, 346, L5.
- Giovanelli, R., Williams, J. P., & Haynes, M. P. 1991, AJ, 101, 1242.
- Giovanelli, R., Haynes, M. P., Kent, B. R., et al. 2007, AJ, 133, 2569.
- Gooch, R. 1996, Astronomical Data Analysis Software and Systems V, 80.
- Haynes, M. P., Giovanelli, R., & Kent, B. R. 2007, ApJ, 665, L19.
- Haynes, M. P., Giovanelli, R., Kent, B. R., et al. 2018, ApJ, 861, 49.
- Heiles, C., Perillat, P., Nolan, M., et al. 2001, Publications of the Astronomical Society of the Pacific, 113, 1247.
- Heiles, C. 2004, GALFA tech. memo 2004-02, [http://www.naic.edu/alfa/memos/general/alfa\\_bm2.ps](http://www.naic.edu/alfa/memos/general/alfa_bm2.ps)

- Helou, G., Hoffman, G. L., & Salpeter, E. E. 1984, *The Astrophysical Journal Supplement Series*, 55, 433.
- Impey, C., Bothun, G., Malin, D., et al. 1990, *ApJ*, 351, L33.
- Kenney, J. D. P., & Koopmann, R. A. 1999, *AJ*, 117, 181.
- Kenney, J. D. P., van Gorkom, J. H., & Vollmer, B. 2004, *AJ*, 127, 3361.
- Kent, B. R., Giovanelli, R., Haynes, M. P., et al. 2007, *ApJ*, 665, L15.
- Kent, B. R., Giovanelli, R., Haynes, M. P., et al. 2008, *AJ*, 136, 713.
- Kent, B. R., Spekkens, K., Giovanelli, R., et al. 2009, *ApJ*, 691, 1595.
- Köppen, J., Jáchym, P., Taylor, R., et al. 2018, *MNRAS*, 479, 4367.
- Koribalski, B. S., Staveley-Smith, L., Kilborn, V. A., et al. 2004, *AJ*, 128, 16.
- Matsuoka, Y., Ienaka, N., Oyabu, S., et al. 2012, *AJ*, 144, 159.
- McMahon, R. G., Irwin, M. J., Giovanelli, R., et al. 1990, *ApJ*, 359, 302.
- Minchin, R., Davies, J., Disney, M., et al. 2005, *ApJ*, 622, L21.
- Minchin, R., Davies, J., Disney, M., et al. 2007, *ApJ*, 670, 1056.
- Peek, J. E. G., Heiles, C., Douglas, K. A., et al. 2011, *The Astrophysical Journal Supplement Series*, 194, 20.
- Roediger, E., & Brüggen, M. 2007, *MNRAS*, 388, 465.
- Salzer, J. J., di Serego Alighieri, S., Matteucci, F., et al. 1991, *AJ*, 101, 1258.
- Sault, R. J., Teuben, P. J., & Wright, M. C. H. 1995, *Astronomical Data Analysis Software and Systems IV*, 433.
- Solanes, J. M., Giovanelli, R., & Haynes, M. P. 1996, *ApJ*, 461, 609.
- Sorgho, A., Hess, K., Carignan, C., et al. 2017, *MNRAS*, 464, 530.
- Matsuoka, Y., Ienaka, N., Oyabu, S., et al. 2012, *AJ*, 144, 159.
- Taylor, R., Davies, J. I., Auld, R., et al. 2013, *MNRAS*, 428, 459.
- Taylor, R., Davies, J. I., Jáchym, P., et al. 2017, *MNRAS*, 467, 3648.
- Turner, N. J. J., & MacFadyen, A. 1997, *MNRAS*, 285, 125.
- Vollmer, B., Beck, R., Kenney, J. D. P., et al. 2004, *AJ*, 127, 3375.
- Vollmer, B., Soida, M., Otmianowska-Mazur, K., et al. 2006, *A&A*, 453, 883.